Supplementary Materials for

Strategy-Dependent Encoding of Planned Arm Movements in Dorsal Premotor Cortex

Thomas M. Pearce and Daniel W. Moran*

correspondence to: dmoran@wustl.edu

This PDF file includes:

Materials and Methods

Animal use

All experiments were carried out following the guidelines of the NIH and Washington University in St Louis Animal Care Committee.

Virtual reality workspace

Reaching tasks were carried out in a virtual reality setup (Fig. S1A). The 3D position of the freely-moving, unconstrained hand was projected onto a 2D fronto-parallel plane and used to control a spherical cursor (radius = 7mm for monkey G; 8mm for monkey H). The workspace was centered such that the cursor was at (0,0) when the hand was in line with the shoulder, with an approximately 90° bend at the elbow. This configuration allowed the monkeys to reach comfortably to all targets while keeping the optoelectric marker in view of the camera system.

Center-out task

The center target (starting position) for each trial was at one of five possible positions: (0,0) or in one of the four quadrants in the planar workspace. The x and y coordinates of these locations were ±40mm (monkey G; monkey H ±35mm). The eight peripheral targets were arranged every 45° around a circle of radius 60mm (monkey G; monkey H 50mm) centered on the starting position for the reach. Center and peripheral targets were 8mm in radius. Each block of movements consisted of 40 successful movements (5 centers x 8 targets), pseudorandomly ordered.

Each center-out trial began when the cursor first touched the randomly-chosen center target. A detailed timeline is shown in fig. S1B. After a fixed-length (500ms) initial delay period, the peripheral target was displayed, beginning a random-length second delay period (500-1300ms, drawn from a uniform distribution). Following this random delay, the center target was extinguished, signaling the "go" cue. The monkey was given 5s to complete the movement. Upon reaching the peripheral target, a 500ms final hold period was started. A small liquid reward was delivered upon successful completion of each trial. Failure to hold at the center until the go cue and failure to reach the target in the allotted time were considered errors; those trials were excluded from the single-unit and population analyses in this study.

Obstacle-avoidance task

The center target was always located at (0,0) and peripheral targets were arranged every 45° on a circle of radius 80mm. The cursor, center and peripheral target dimensions were unchanged from the center-out task. The virtual obstacle consisted of a three-sided box surrounding the center target. The perpendicular distances from (0,0) to the bottom (opposite the opening) and sides of the box were 25mm and 24mm respectively. The direction from (0,0) to the middle of the open side was considered the obstacle direction. For each target direction, the obstacle could be in the same direction (0° condition, straight reach required), rotated ±90° or ±135° (Fig. 1E). 8 targets x 5 relative orientations of the obstacle = 40 conditions. In addition, catch-trials with no obstacle were performed. Each block of movements consisted of 48 successful movements (the 40 distinct obstacle conditions + 8 catch trials, one for each target), pseudorandomly ordered.

Each obstacle-avoidance trial began when the cursor first touched the center target. A detailed timeline is shown in fig. S1C. After a fixed-length (500ms) initial delay period, the peripheral target was displayed, beginning a second fixed length delay period (also 500ms), at the end of which either an obstacle was displayed (5/6 of total) or the "go" cue was given (catch-trials, 1/6 of total). For non-catch-trials, a random-length third delay was then started (500-1300ms, drawn from a uniform distribution). Following this random delay, the center target was extinguished, signaling the "go" cue. The monkey was given 5s to complete the movement. Upon reaching the peripheral target, a 500ms final hold period was started. A small liquid reward was delivered upon successful completion of each trial. Failure to hold at the center until the go cue, contact between the cursor and the obstacle, and failure to reach the target in the allotted time were considered errors; those trials were excluded from the single-unit and population analyses in this study.

Neural data acquisition

Extracellular recordings were made using glass/tungsten microelectrodes, from a cylindrical chamber centered at 19mm anterior, 14mm lateral in interaural stereotactic coordinates. Electrodes were driven until spiking activity was seen, then left for the duration of a session. Multiple sessions at different cortical depths were performed daily. Recordings were bandpass-filtered (300-5000 Hz), pre-amplified, and digitally sampled at 24,414 Hz. Single units were identified using a Matlab-based offline spike sorter (*30*). Units were not screened for task- or reach-related activity; rather, while the monkey was at rest, electrodes were driven until spiking activity was seen and not moved for the duration of the behavioral session. All units which remained stable for the duration of the session were included in the analysis, minimizing selection bias in the population of recorded neurons. Two recording sessions per penetration site were performed, with the electrodes advanced at least 0.25mm deeper between sessions.

Single unit tuning analysis

Two-dimensional multiple linear regressions were used to quantify cosine tuning properties.

R: firing rate estimate for each trial; $(\text{spikes/s})^{0.5}$

$P_{x,y}$: coordinates of the parameter of interest

b: regression coefficients

$R = b_1*P_x + b_2*P_y + b_3$

Single-bin regression analysis

Position regression (center-out task): $P_{x,y}$ are the coordinates of the initial hold position. R is the single-bin rate during the time window 150-650 ms after the center target was touched (Fig. S1B, red line).

Initial velocity/target regression (center-out task): $P_{x,y}$ are the coordinates of the peripheral target relative to the initial hold position. R is the single-bin rate during the time window 150-650 ms after the peripheral target was displayed (Fig. S1B, green line).

Initial velocity regression (obstacle-avoidance task): $P_{x,y}$ are the coordinates of the center of the obstacle opening. R is the single-bin rate during the time window 150-650 ms after the obstacle was displayed (Fig. S1C, orange line).

Target regression (obstacle-avoidance task): $P_{x,y}$ are the coordinates of the peripheral target. R is the single-bin rate during the time window 300-800 ms after the obstacle was displayed (Fig. S1C, blue line).

Temporally-resolved regression analysis

The same procedure was used as with the single-bin analysis, but smoothed estimates of the instantaneous firing rate were calculated by convolving the spike train with a Gaussian kernel (s.d. = 66ms).

Square-root transform

In both single-bin and temporally-resolved regression analyses, the firing rates were square root transformed to stabilize variance so that parametric statistical tests of the significance of the cosine fit could be performed (*31*). We also performed regression analyses on the raw, untransformed firing rates, and confirmed that the distribution of preferred directions in the two cases was largely unaffected by the transform, and did not affect the interpretation of the findings in this study.

Population vector analysis

The PV models were built using the regression coefficients from single-bin analyses (see above). In an effort to avoid arbitrary decisions regarding inclusion criteria, all recorded units were used in the population decoders regardless of the significance of tuning. For this reason, we did not normalize the preferred direction/position vectors (i.e. the regression coefficients) to unit length. This provides higher weights (i.e. Euclidean length) to units with strong tuning, and lower weights to those with weak tuning or very low rate, which contribute noisier signal. The indirect optimal linear estimator method (*19*) was then used to compute population vectors as follows:

n: number of neurons in model

t: time points being decoded

E [t x 2]: estimate of a particular parameter (position, velocity, or target)

R [t x n]: z-score normalization of instantaneous firing rate estimates

B [n x 2]: encoding vectors (coefficients b_1, b_2 from single-unit regression analysis)

W [n x 2]: decoding vectors or weights;

M^{-1} is the matrix inverse of a matrix M

M^{+} is pseudoinverse of a matrix

M' is the transpose of a matrix

Decoding vectors W are calculated from encoding vectors B:

$W = (B^{+})' = B\,[(B'B)^{-1}]'$

Neural population estimates E are calculated from decoding vectors W and measured rates R:

E [t x 2] = R [t x n] W [n x 2]

Models were tested by decoding the estimated instantaneous firing rate measured during the obstacle-avoidance task. The rate estimates for each neuron were z-score normalized across all successful trials. Two of the three models (position and target-direction regressions from the center-out task delay periods) were built from tuning

during the center-out task, so testing on the obstacle-avoidance task was a completely independent data set. The results of these PV analyses are shown in Figs. 2-3 and Figs. S2-S3. The third model was constructed from target-tuning regressions during the final delay period of the obstacle-avoidance task. Since the encoding and decoding were done from the same task, a leave-one-out cross-validation was used to avoid building and testing on the same data. In this method, each trial was considered independently; the regression coefficients used in the decoder were calculated from the remaining 199 trials. This procedure was repeated for all trials. The target-based PV analyses in this paper (Figs. S4-S5) were all calculated using leave-one-out regression models. We also performed the analyses without a cross-validation (including all 200 trials in the regression), and leaving out all trials of a particular target-obstacle condition (including 195 trials in the regression, and testing on the other 5). The results of these analyses were not significantly different than the leave-one-out results.

To determine the magnitude at which a PV should be considered significant, we utilized a bootstrap technique. The firing rates were randomly resampled and multiplied by the real decoding matrix W to create a distribution of PVs obtained when the relationship between firing rate and trial type was due to chance alone. The magnitudes were then sorted and the 95^{th} percentile was used as a p=0.05 significance threshold (Fig. 3 and fig. S5). As an illustration of the statistical properties of PV length, consider the initial period of each trial. Prior to the first display of the target on each trial, the magnitudes of the velocity and target PV decoders are small and the directions are unstable, which is to be expected, as no information about the upcoming movement is available to the subject. As visual information becomes available over the course of the trial, the PV lengthens and the direction stabilizes.

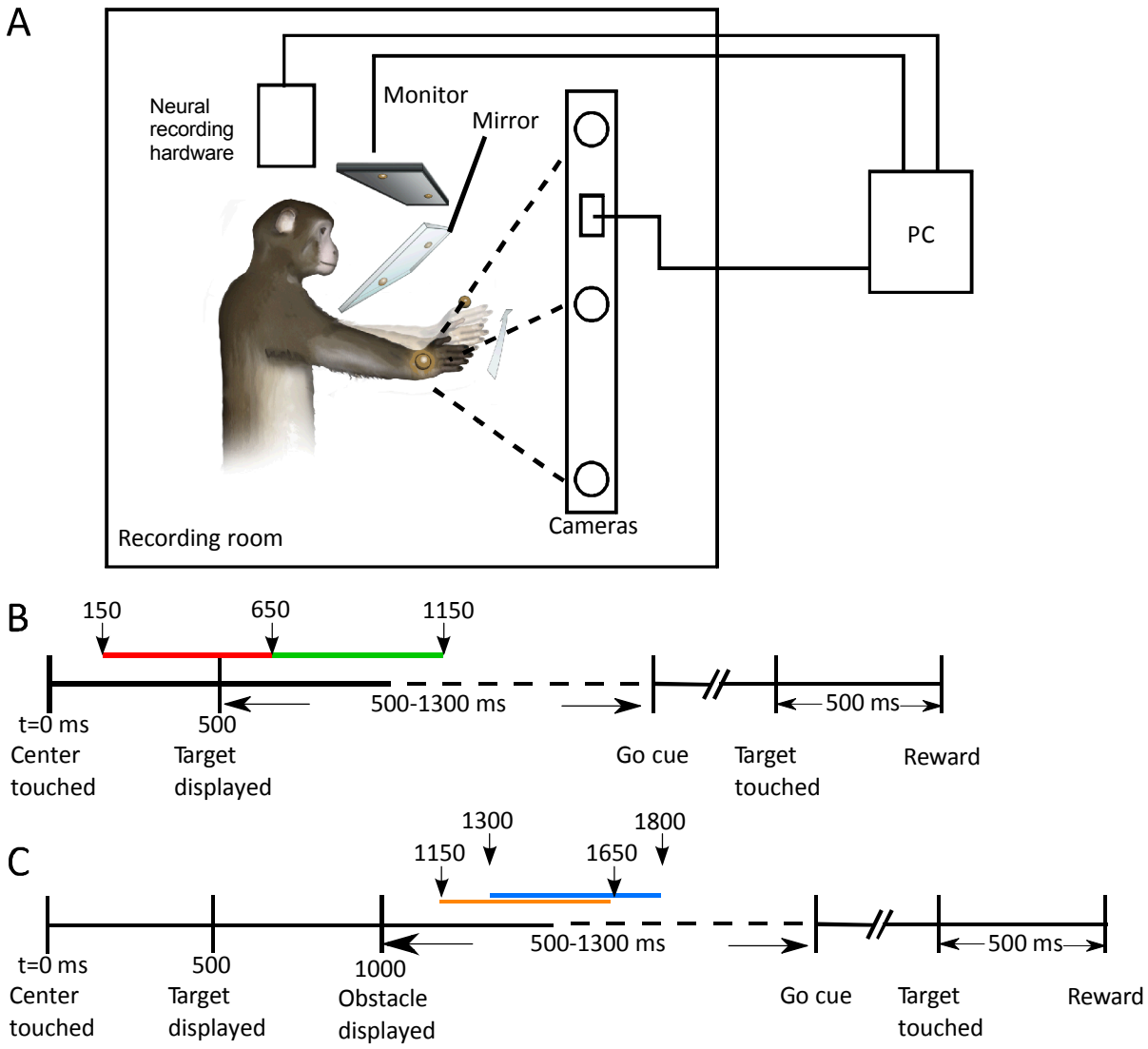

Fig. S1.

Experimental setup. A) The monkeys sat in a primate chair with the arm ipsilateral to the recording chamber restrained. An optoelectric marker was located on the dorsum of the hand contralateral to the chamber. The position of this marker was recorded by a camera system and sent to a PC. Movements were unconstrained and occurred in 3D space. The position of the hand was mapped onto the frontal plane and used to control the cursor in a 2D workspace. Only this virtual-reality workspace was visible to the monkey; the hand was obscured by a mirror. B) Detailed timeline of a center-out trial. Position regressions were performed using the firing rate from 150 to 650 ms after the initial position was reached (red line). Initial velocity regressions were performed using the firing rate from 150 to 650 ms after the target was displayed (green line). C) Detailed timeline of an obstacle-avoidance trial. Initial velocity regressions were performed using the firing rate from 150-650 ms after the obstacle was displayed (orange line). Target/goal direction regressions were performed using the firing rate from 300-800 ms after the obstacle was shown (blue line).

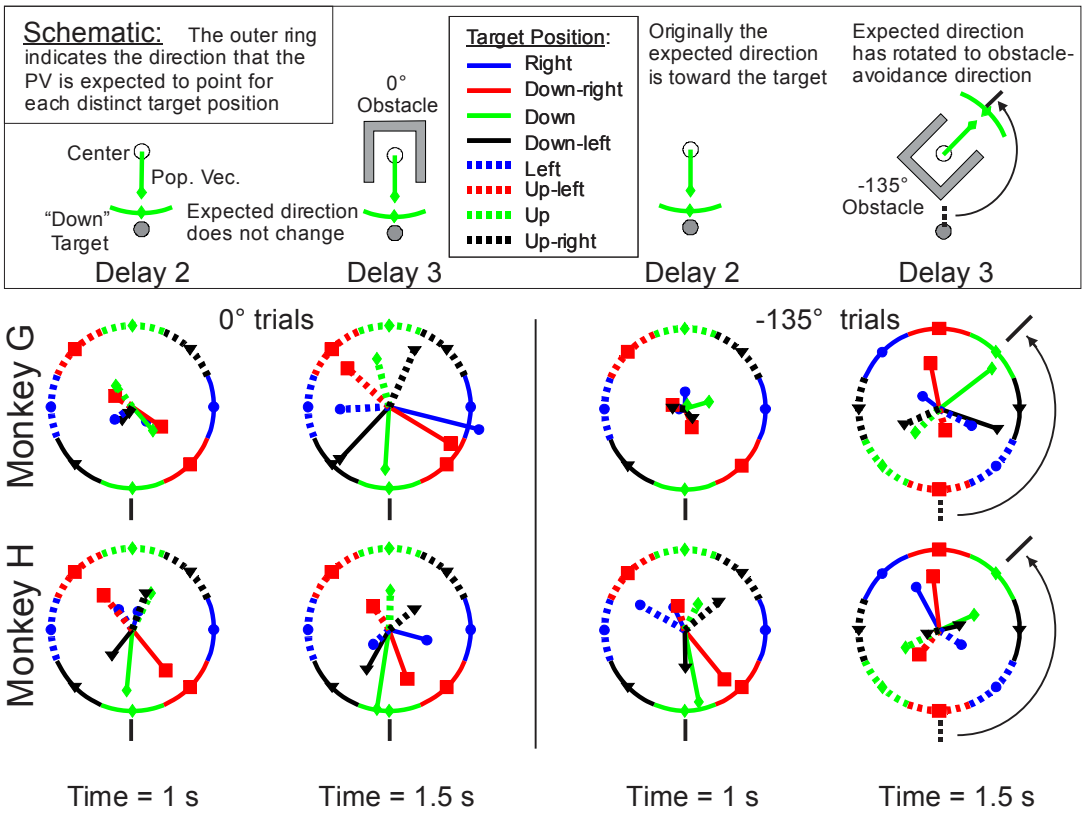

Fig. S2

Population vector (PV) performance to individual targets for two relative obstacle orientations. The velocity-based PVs are decoded from neural activity for 5 repetitions to each of the 8 targets. This is in contrast to the other PV-related figures (Figs. 2-3, S4-S5) where data were rotationally collapsed across trials with the same relative orientation of target and obstacle. Top: schematic illustration of a PV to a single target, for two obstacle conditions. The vector originates from the "center" circle, where the hand is located during the delay periods. The arc with matching color and line style indicates the direction the PV is expected to point based on the information available in each epoch. Bottom: PVs from monkeys G and H. All 8 target conditions are shown for 0° (left) and -135° (right) relative obstacle orientations. Time = 1 s occurs at the end of delay 2, immediately prior to obstacle onset while time = 1.5 s occurs 500 ms after obstacle appearance. In both the 0° and -135° trials, monkey G waits for the obstacle information to appear before developing significant length in the population vectors. Monkey H, in contrast, develops significant populations pointing to the target at time = 1s. By time = 1.5s, monkey H has rotated these vectors to the appropriate obstacle exit direction.

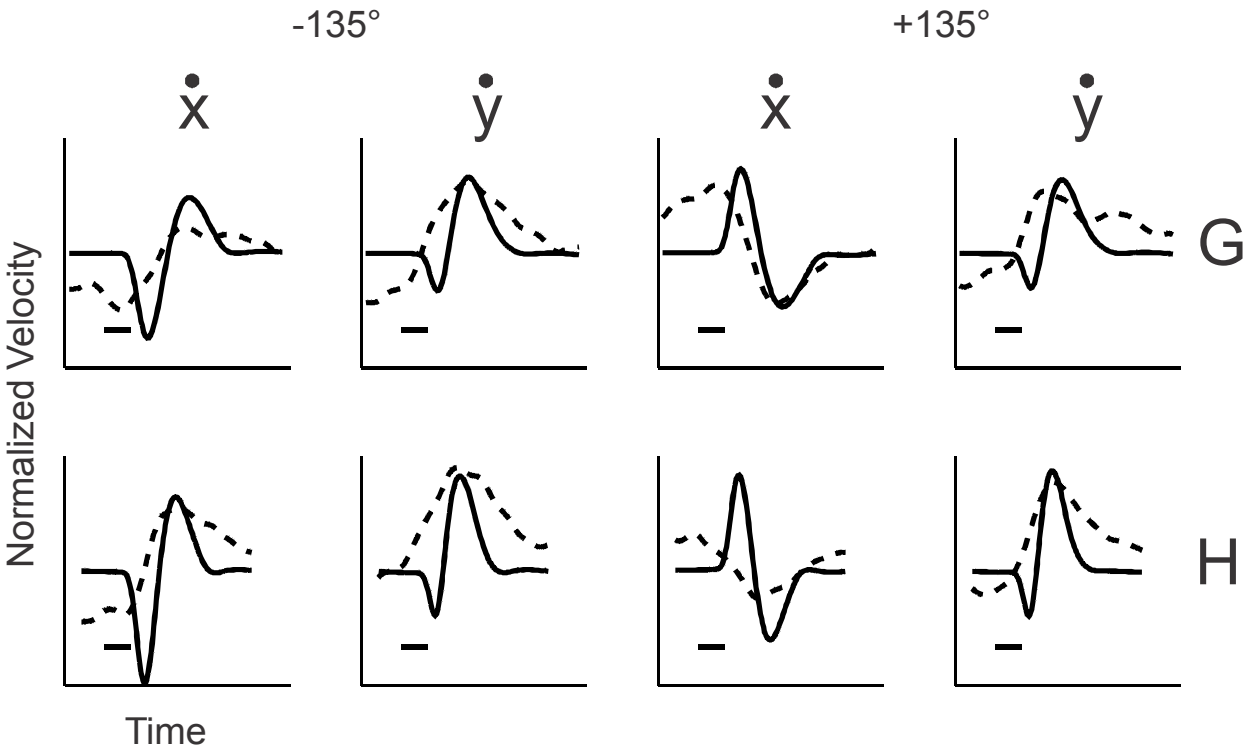

Fig. S3

Decoding velocity during the movement period. *x* and *y* component velocities are shown for the ±135° conditions (the same conditions as in Fig. 1 F-G for the position decoder) for monkey G (top) and monkey H (bottom). Solid lines are the average velocities of the recorded kinematics, while dashed lines are the PV-decoded velocity estimates. A relationship exists but is weaker than that seen for the decoded hand positions (Fig. 1 E-G). Scale bars: 200ms.

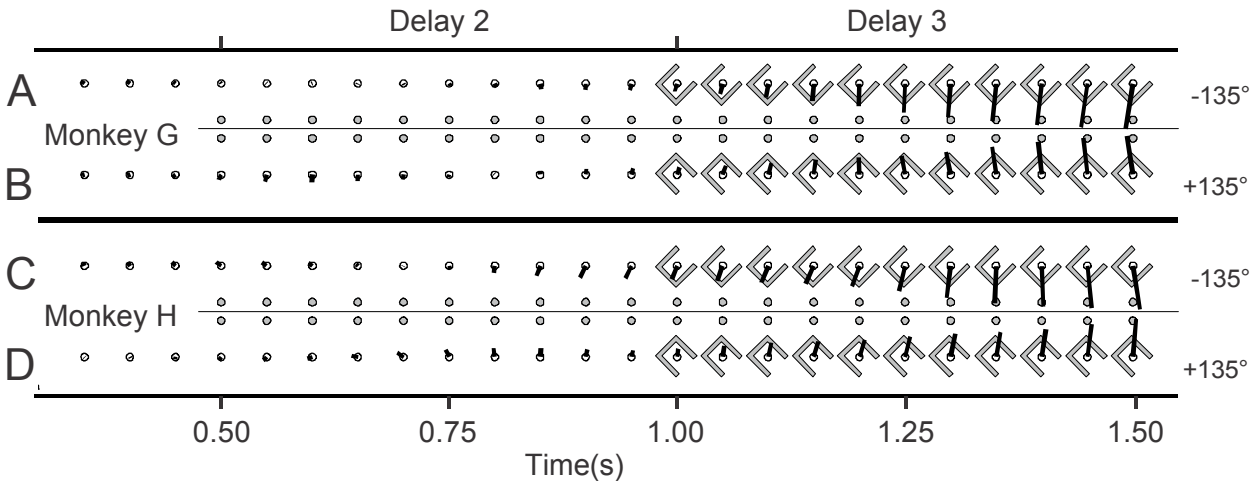

Fig. S4

The target-based PV predicts target direction regardless of the initial movement direction. A-B) Monkey G, ±135° trials. Task visualization and decoded vector are shown every 50ms. C-D) Same as A-B, for monkey H.

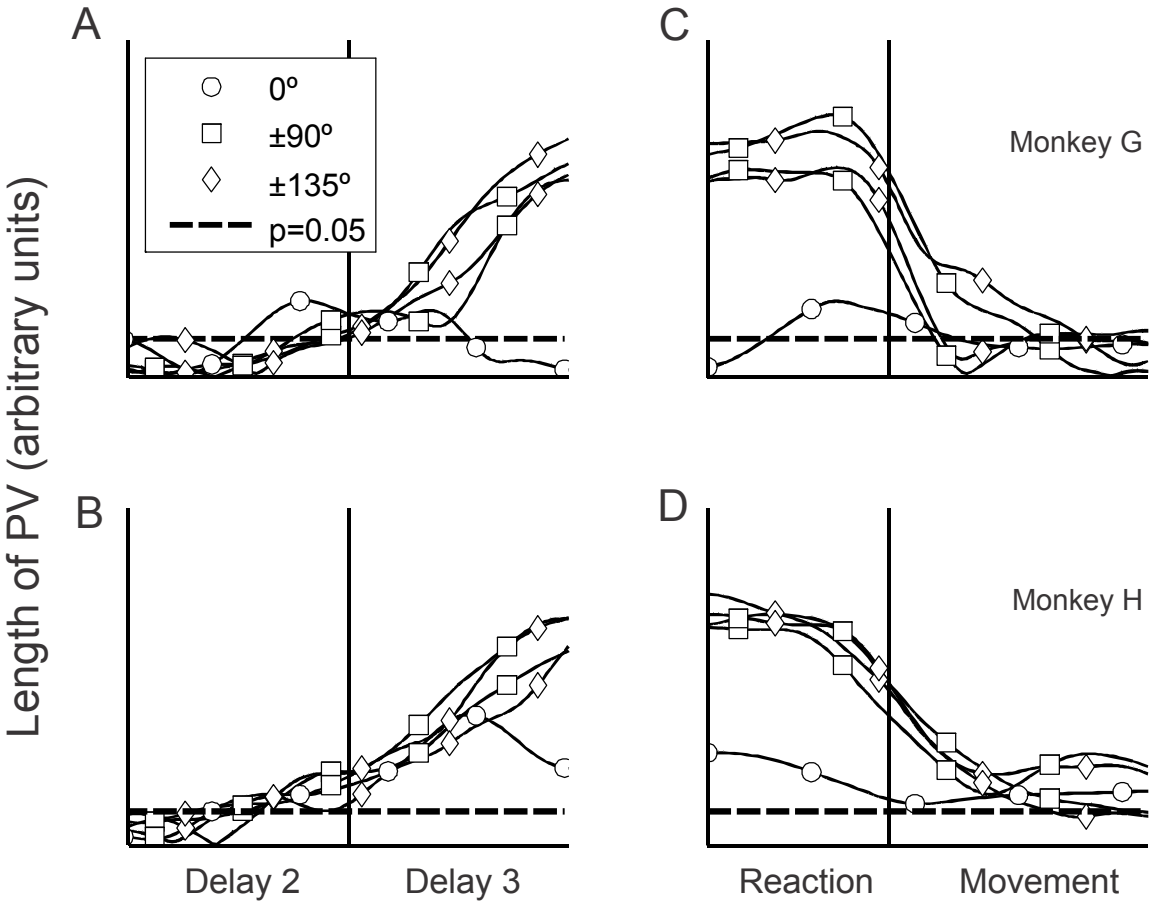

Fig. S5

Length of the target-based PV as a function of time. A-B) PV length during the delay periods for monkeys G and H respectively. C-D) Same as A-B, during reaction and movement times. Note that the vector for the 0° condition is reduced in length compared to the other conditions, where the obstacle impedes a straight reach.

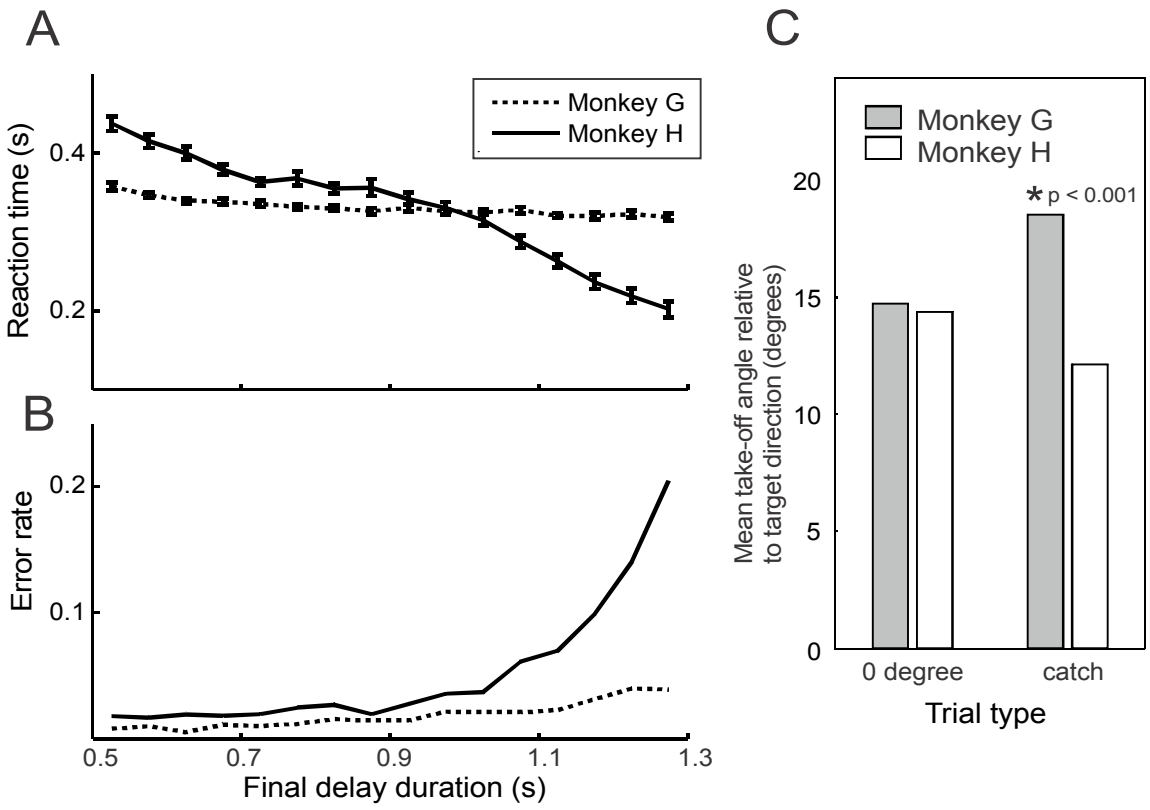

Fig. S6

Behavioral evidence of different planning strategies on the obstacle-avoidance task. A) Reaction time (mean ± SEM) as a function of random delay length. Monkey G reacted with nearly the same response time for the shortest and longest delays, while monkey H appeared to be attempting to anticipate the occurrence of the "GO" cue. B) Error rate as a function of random delay length. Monkey H was substantially more likely to make reaction-time errors (moving before the "GO" cue) for the longest of the random delays. C) Mean angle at movement onset between the hand and target directions for two trial types. For direct (0°) trials, the obstacle was present but did not impede a straight path to the target. Catch-trials had no obstacle, and the "GO" cue was given 500ms after the target onset, at the time when the obstacle would usually be displayed. At that time, the velocity-based PV for monkey H was significant, while that for monkey G was not. Accuracy on catch-trials was significantly different ($p < 0.001$ using both the parametric k-test, a test for equal concentration parameters of von Mises distributions, and the non-parametric Kuiper's test (*32*).